SEASONAL AND DIURNAL VARIATION IN THE VERTICAL STRUCTURE OF THE MARTIAN NITRIC OXIDE NIGHTGLOW LAYER

Zachariah Milby, Nicholas M. Schneider, Sonal K. Jain, Kyle Connour, *LASP, U. Colorado, USA (nick.schneider@lasp.colorado.edu)* **Francisco González-Galindo**, *Instituto de Astrofísica de Andalucía (IAA-CSIC),* Granada, Spain, **Franck Lefèvre**, *Laboratoire Atmosphères, Milieux, Observations Spatiales (LATMOS)*, *CNRS*, *Sorbonne Université*, *UVSQ*, Paris, France, **François Forget**, *Laboratoire de Météorologie Dynamique/IPSL*, *Institut Universitaire de France*, *Sorbonne Université*, *École Normale*, **Jean-Claude Gérard**, *Laboratoire de Physique Atmosphérique et Planétaire (LPAP), Université de Liège*, Liège, Belgium

Introduction:

Nitric oxide (NO) nightglow is an emission feature that can provide insight into the dynamics of the Martian middle atmosphere (Figure 1). It is an atmospheric airglow phenomenon produced by the chemi-luminescent relaxation of excited NO molecules and is the brightest middle-ultraviolet (MUV) spectral feature in the Martian nightside atmosphere, with the occasional exception of aurora (Schneider et al., 2018). NO forms when carbon dioxide and molecular nitrogen dissociate on the dayside, the atoms get transported to the nightside and the resultant nitrogen and oxygen recombine. The reaction leaves the resulting molecule in an excited state which decays radiatively by giving off one photon. Because the brightness is proportional to the recombination rate of nitrogen and oxygen atoms, it responds to the dayside photo-dissociation rates of carbon dioxide (CO) and molecular nitrogen (N2), to Hadley circulation from the dayside to the nightside and to local downward flux into the lower atmosphere (Schneider et al., 2020). It is a phenomenon distinct from NO dayglow, a solar-driven fluorescence proportional to the number density of NO molecules rather than an instantaneous reaction rate (Stevens et al., 2019).

The first observations of NO nightglow on Mars came from data obtained by the Spectroscopy for the Investigation of the Characteristics of the Atmosphere of Mars (SPICAM) instrument on the Mars Express (MEx) spacecraft. Bertaux et al. (2005) reported the first detection of NO nightglow in Mars year (MY) 32 during southern hemisphere winter. They interpreted their results using simulations from the LMD-MGCM and proposed that the density of nitrogen is the limiting factor for NO nightglow emission because it is predicted to be orders-of-magnitude lower in abundance than that of oxygen. SPICAM-based studies by Cox et al. (2008) analyzed vertical profiles with a 1-D model, showing that they could be adequately explained by downwelling of atomic species or by eddy diffusion. They also confirmed model predictions that the southern winter pole would be brighter with a lower altitude emission peak. Further studies by Gagné et al. (2013) and Stiepen et al. (2015) analyzed nightglow observations from additional orbits, but were hindered in their statistical analyses by the limited dataset.

Methods:

We performed a comprehensive study of the variability of Martian nitric oxide (NO) nightglow's brightness and altitude. We used MAVEN Imaging Ultraviolet Spectrograph (IUVS) limb data gathered between Mars years 32 and 36. The IUVS instrument is an imaging slit spectrograph with a scanning mirror that moves perpendicular to the slit, gathering spectral information with two spatial axes. The NO nightglow band system is captured by the MUV detector which has a wavelength range of 175 to 340 nm, a spectral resolution of 0.65 nm and good sensitivity over the wavelengths with the strongest NO nightglow bands. MAVEN's eccentric orbit slowly evolves in latitude and local time, giving IUVS the ability to collect data over a wide range of physical conditions unavailable to previous studies. During limb observations the motion of the scanning mirror generates vertical profiles, capturing spectra at different altitudes (Jain et al., 2015). In addition to the limb scans obtained during periapse passage (used in (Stiepen et al., 2017)), we use limb scans obtained from the inbound and outboard orbit segments just before and after periapse.

General circulation models (GCMs) provide insights regarding the middle atmosphere and NO nightglow. GCMs are the primary way by which we understand the Martian middle atmosphere, as previous observations of this region are limited (Barnes et al., 2017); consequently, any observational constraints we can provide will help further refine the insights they provide. Previous studies of the Martian NO nightglow (Bertaux et al., 2005; Gagné et al., 2013; Stiepen et al., 2015, 2017; Schneider et al., 2020) interpreted their results using *Laboratoire de Météorologie Dynamique* Mars GCM (LMD-MGCM) simulations. While many aspects of nightglow are matched by the model, persistent discrepancies remain. Most of these previous studies found that the simulations did not accurately predict some of the observed characteristics of the nightglow layer—the model almost always predicted the peak altitude of the layer to be tens of kilometers higher and around half as bright as observations indicated.

The model is apparently underestimating some key physical components, or otherwise incorrectly accounting for NO nightglow, that may have implications for the broader planetary circulation.

Results:

We investigated how the nightglow varied with latitude and season. Our multi-year analysis showed no systematic year-to-year variability of the NO peak brightness or altitude. We found that in low-to-mid latitudes, the nightglow was significantly brighter and found at lower altitudes in the aphelion season than the perihelion season. The nightglow was significantly brighter over the winter poles, with the north pole being the brightest and peaking at lower altitudes than than the southern pole. This confirms the latitude-dependence in peak altitude and peak brightness reported by Stiepen et al. (2017) and Schneider et al. (2020), though with additional coverage. Our model simulations occasionally agreed with these observations but generally underpredicted the brightnesses. They consistently produced peak brightnesses 15–20 km higher than our observations.

We also explored the diurnal cycle of the nightglow. Our observations suggest the mesosphere is relatively steady during the aphelion season. The perihelion season was more dynamic, producing a near-midnight enhancement in the brightness. Our simulations did not predict the relatively calm aphelion season that we observed. They produced some of the features we observed during the perihelion season but most notably did not predict the local time ehancement that we noticed.

Atmospheric tides are an insightful metric for identifying atmospheric forcings and revealing how the atmosphere has responded. Stiepen et al. (2017) first reported the detection of a wave-3 structure in the peak brightness of the nightglow. Schneider et al. (2020) were able to detect similar waves and analyzed them using the broad spatial and temporal coverage of the imaging data. They interpreted their results using LMD-MGCM simulations and they determined the waves to be primarily diurnal, non-migrating eastward-propagating wave-2 structures (called DE2) with a small semi-diurnal westward-propagating wave-1 component (SW1). The central peak of their observed equatorial wave structure moved eastward at a rate of 4.7°h−1.

Figure 2 (a) shows a pronounced wave-3 structure in the peak limb brightness between −45° and 45° latitude, smoothed in longitude by a 30°-wide kernel. This confirms the existence of the waves reported by (Stiepen et al., 2017) and Schneider et al. (2020). We used least-squares fits to the peaks of the waves to calculate an average eastward wave motion of 4.2 ± 0.8 ° h−1. Note that unlike previous statistics in this paper this uncertainty represents the error in the fit rather than geophysical variation in the longitude of the observations. This wave speed is slightly faster than the one reported by Schneider et al. (2020), but within one standard deviation, and both are consistent with the DE2 wave. The peaks were also at approximately the same planetary longitudes and the wave near 0° longitude exhibits the largest fractional deviation in the early evening hours, suggesting we were able to detect the same equatorial wave structures in the limb observations. The simulations in figure 2 (b) show a wave-3 structure as well. However, the simulated wave propagates eastward at a slower 3.3 ± 0.9 ° h−1 and doesn't exhibit the same peak brightness near 0° longitude in the observations.

We also observed a remarkable wave-3 structure in the altitude of the peak limb brightness (Figure 2b), also smoothed in longitude by the same 30°-wide kernel as the brightness. The maxima of the wave structures in (a) and (b) do not coincide, but appear appear to be offset from each other by about 45°. This offset of the waves is especially noticeable in figure 2 (c) which shows the wave structures corrected for the 5 ° h−1 DE2 wave motion by removing the longitudinal shift relative to midnight. If brightness and altitude were perfectly correlated or anticorrelated, first-order explanations might present themselves. But the 45° shift suggests a complex interplay of multiple dynamical influences. Unfortunately, the model does not replicate much of the wave-3 structure let alone its amplitude, so this leaves a challenge for future modelers.

References:

Bertaux, J.-L., et al., (2005). *Science*, *307*(5709), 566–569. doi: 10.1126/science.1106957

Cox, C., et al. (2008). *Journal of Geophysical Research*, *113*(E8). doi: 10.1029/2007je003037

Gagné, M.-È., et al.. (2013). *Journal of Geophysical Research: Planets*, *118*(10), 2172–2179. doi: 10.1002/jgre.20165

Jain, S. K., et al. (2015). *Geophysical Research Letters*, *42*(21), 9023– 9030. doi: 10.1002/2015gl065419

Schneider, N. M., et al. (2020). *Journal of Geophysical Research: Space Physics*, *125* (e2019JA027318). doi: 10.1029/2019ja027318

Stiepen, A., et al. (2015). *Geophysical Research Letters*, *42*(3), 720–725. doi: 10.1002/2014gl062300

Stiepen, A., et al. (2017). *Journal of Geophysical Research: Space Physics*, *122*(5), 5782–5797. doi: 10.1002/2016ja023523

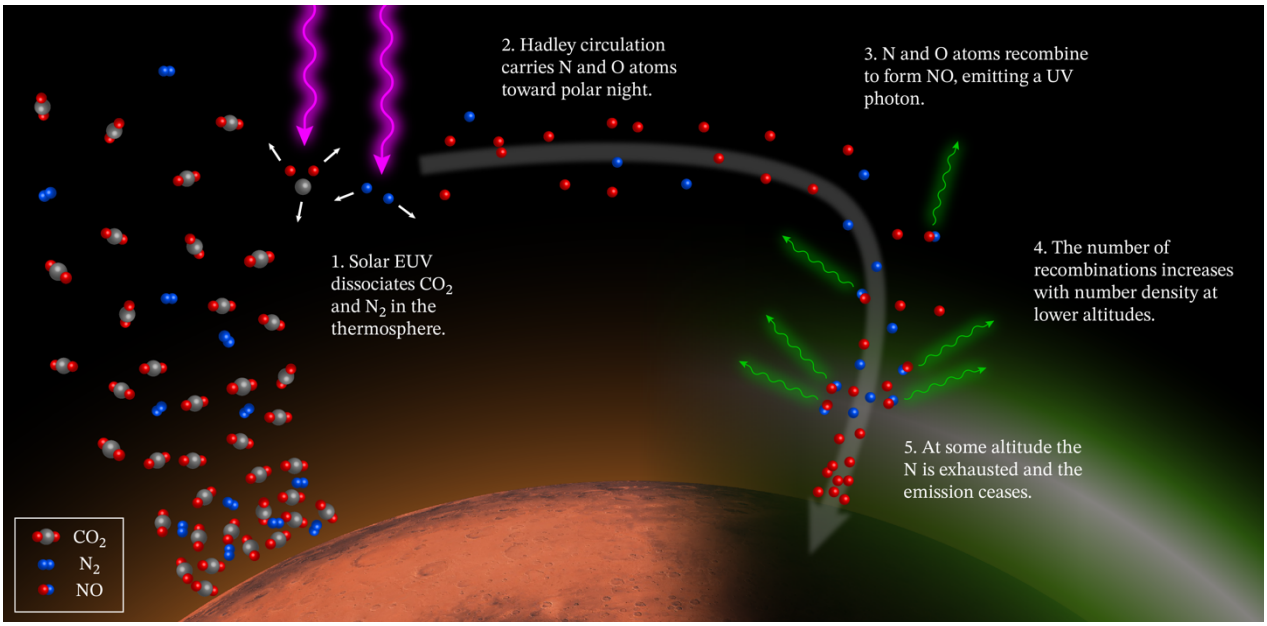

Figure 1. The NO nightglow recombination process.

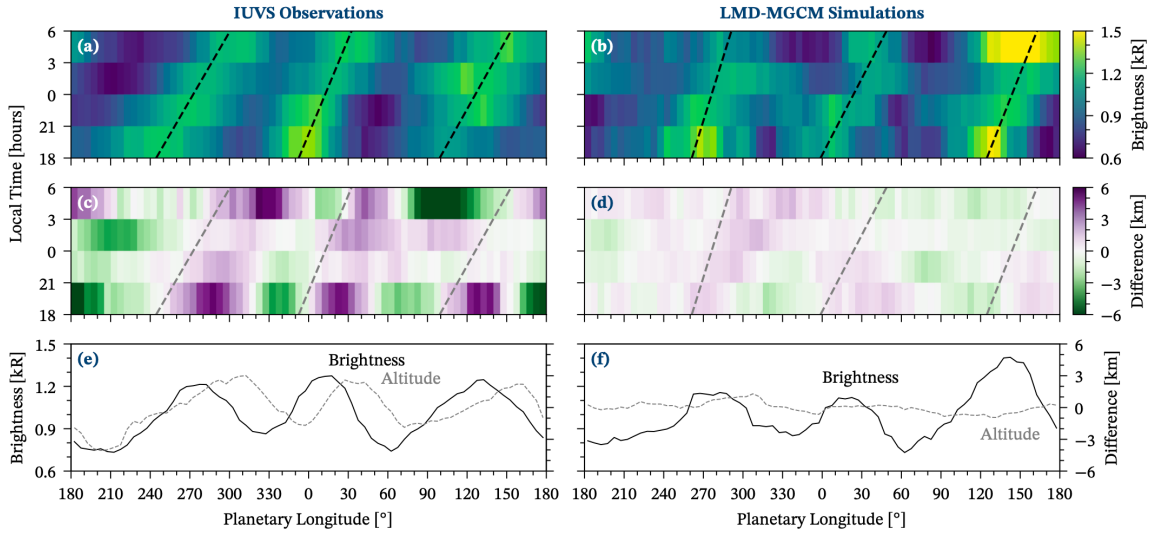

Figure 2. Wave propagation with local time between −45° and 45° latitude. (a) shows observed peak limb brightness for a given local time bin and (b) shows the same for the simulations. In both, dashed lines show fits to the peak brightnesses (c) shows the absolute difference from the average peak altitude and (d) shows the same for the simulations. The grey dashed lines are replicated from the panels above, showing the peak brightness and altitude are out of phase. (e) shows the brightness and altitude data from (a) and (c) averaged across all local times, normalized and corrected for DE2 wave motion by removing the longitudinal shift relative to midnight. (f) shows the same for the simulations in (b) and (d).